Langmuir
Article
pubs.acs.org/Langmuir

Experimental and Numerical Study of Spread and Sorption of VX Sessile Droplets into Medium Grain-Size Sand

Terrence G. D'Onofrio,*[,†] Homayun K. Navaz,[‡] Bojan Markicevic,[‡] Brent A. Mantooth,[†] and Kenneth B. Sumpter[†]

[†]*Department of the Army, Edgewood Chemical Biological Center (ECBC) Aberdeen Proving Ground, Maryland 21010 and* [‡]*Kettering University, Department of Mechanical Engineering 1700 University Avenue, Flint, Michigan 48504*

Received August 17, 2009. Revised Manuscript Received November 2, 2009

The experimental measurement and modeling of liquid chemical agent spread and sorption on a porous substrate are described. Experimental results with the nerve agent *O*-ethyl *S*-(2-diisopropylaminoethyl) methylphosphonothiolate (VX) demonstrate that the wetted imprint volume increases, even after the sessile drop volume is exhausted. This indicates the wetted imprint is only partially saturated, and a multiphase flow problem formulation is needed to predict the VX fate in porous substrates. Three characteristics and their changes in time: (i) sessile volume remaining, (ii) wetted imprint area on the sand surface where the droplet is deposited, and (iii) VX penetration depth into sand, are computed numerically and compared to experimentally measured values. A very good qualitative and quantitative agreement was found between the numerical and experimental results. These numerical and experimental methods can be used to determine the spread and sorption of hazardous materials into a variety of substrates.

1. Introduction

The interactions between a liquid and a substrate are an important factor in determining the overall fate of the liquid. In the case of a liquid deposited onto porous substrates, the droplets sorb into the substrate, from where they may evaporate, react, or be sequestered.[1−3] Previous studies of the sessile droplet fate have mainly addressed the sorption time and spread during periods when there is sessile volume present at the porous medium surface. The sorption time and the shapes of the sessile-drop volume, and the wetted imprint have been predicted using analytical models[4,5] and numerical simulations.[6,7] In these models, the capillary pressure at the free interface is obtained from the Washburn equation, and the wetted imprint saturation is set equal to one (i.e., fully saturated).[8] The liquid/substrate interactions influence the sessile volume shape and contact angle,[9,10] where the sorption dynamics may be determined by the liquid slip velocity.[11,12] The wetting influences the capillary force, which is opposed by the drag force of the porous substrate, with the resultant of those forces governing the sorption process.[13]

However, once there is no sessile-drop volume remaining, the liquid can continue to spread into previously dry regions within the porous substrate, thus increasing the wetted volume. Therefore, the wetted volume of porous substrate is not fully saturated by liquid, i.e., the pores are not filled with liquid. Instead, the liquid proceeds along preferential flow paths producing a partially wetted imprint of volume much larger than the fully saturated volume. Along these lines, the sorption times for some pairs of liquid/powders can not be predicted using the fully saturated imprint assumption, indicating the formation of a partially saturated imprint.[14] The experimental evidence from MRI measurements further corroborate this partially saturated imprint multiphase flow.[15−18] Using the capillary network model, Markicevic and Navaz[19] have shown numerically the transition between fully and partially saturated imprint during the droplet sorption. This implies that the droplet sorption should be solved as a multiphase flow problem, with the multiphase flow parameters, capillary pressure and relative permeability[20−22] included in the momentum conservation equation.[23]

*Corresponding author. E-mail: terrence.donofrio@us.army.mil. Telephone: (410) 436-5755. Fax: (410) 436-7129.

(1) Kilpatrick, W. T.; Ling, E. F.; Brevett, C. A. S.; Hin, A. R. T.; Fagan, M. W.; Murdock, W. P., Experimental Design Requirements for Predictive Model Development using Agent Fate Wind Tunnels. *Air Force Research Laboratory Technical Report* **2008**; AFRL-HE-WP-TR-2004.
(2) Savage, J. J. In Agent Fate Program Overview Presented at the 74th Military Operations Research Society Symposium (MORSS); Colorado Springs, CO., **2006**.
(3) Savage, J. J. In Agent Fate Program Overview Presented at the 2006 Scientific Conference on Chemical Biological Defense Research; Hunt Valley, MD, **2006**.
(4) Denesuk, M.; Smith, G. L.; Zelinski, B. J. J.; Kreidl, N. J.; Uhlmann, D. R. *J. Colloid Interface Sci.* **1993**, *158*, 114−120.
(5) Hapgood, K. P.; Litster, J. D.; Biggs, S. R.; Howes, T. *J. Colloid Interface Sci.* **2002**, *253*, 353−366.
(6) Alleborn, N.; Raszillier, H. *Chem. Eng. Sci.* **2004**, *59*, 2071−2088.
(7) Alleborn, N.; Raszillier, H. *J. Colloid Interface Sci.* **2004**, *280*, 449−464.
(8) Washburn, E. W. *Phys. Rev.* **1921**, *17*, 279−283.
(9) Starov, V. M. *Adv. Colloid Interface Sci.* **2004**, *111*, 3−27.
(10) Starov, V. M.; Kostvintsev, S. R.; Sobolev, V. D.; Velarde, M. G.; Zhdanov, S. A. *J. Colloid Interface Sci.* **2002**, *252*, 397−408.
(11) Davis, S. H.; Hocking, L. M. *Phys. Fluids* **1999**, *11*, 48−57.
(12) Davis, S. H.; Hocking, L. M. *Phys. Fluids* **2000**, *11*, 48−57.
(13) Holman, R. K.; Cima, M. J.; Uhland, S. A.; Sachs, E. *J. Colloid Interface Sci.* **2002**, *249*, 432−440.
(14) Popovich, L. L.; Feke, D. L.; Manas-Zloczower, I. *Powder Technol.* **1999**, *104*, 68−74.
(15) Reis, N. C., Jr.; Griffiths, R. F.; Mantle, M. D.; Gladden, L. F. *Int. J. Heat Mass Transfer* **2003**, *46*, 1279−1292.
(16) Brevett, C. A. S.; Cook, C. L.; Nickol, R. G.; Sumpter, K. B.; Hall, M. R., Degradation of Mustard on Moist Sand, Asphalt and Limestone using ^{13}C SSMAS NMR. *Edgewood Biological Chemical Center Technical Report* **2006**, ECBC-TR-523, (U).
(17) Wagner, G. W.; O'Connor, R. J.; Edwards, J. L.; Brevett, C. A. S. *Langmuir* **2004**, *20*, 7146−7150.
(18) Wagner, G. W.; O'Connor, R. J.; Procell, L. R. *Langmuir* **2001**, *17*, 4336−4341.
(19) Markicevic, Bojan; Navaz, Homayun K. *Int. J. Numer. Methods Heat Fluid Flow* **2009**, *19*, 521−534.
(20) Leverett, M. C. *AIME Trans.* **1941**, *142*, 152−169.
(21) Udell, K. S. *Int. J. Heat Mass Transfer* **1985**, *28*, 485−495.
(22) van Genuchten, M. T. *Soil Sci. Soc. Am. J.* **1980**, *44*, 892−898.
(23) Bear, J. *Dynamics of Fluids in Porous Media*; Dover Publications, Inc.: New York, 1988.

 DOI: 10.1021/la903071q

Report Documentation Page

Form Approved
OMB No. 0704-0188

1. REPORT DATE	2. REPORT TYPE	3. DATES COVERED
2009		**00-00-2009 to 00-00-2009**

4. TITLE AND SUBTITLE	5a. CONTRACT NUMBER
Experimental and Numerical Study of Spread and Sorption of VX Sessile Droplets into Medium Grain-Size Sand	5b. GRANT NUMBER
	5c. PROGRAM ELEMENT NUMBER
6. AUTHOR(S)	5d. PROJECT NUMBER
	5e. TASK NUMBER
	5f. WORK UNIT NUMBER
7. PERFORMING ORGANIZATION NAME(S) AND ADDRESS(ES) **Department of the Army,Edgewood Chemical Biological Center (ECBC),Aberdeen Proving Ground,MD,21010**	8. PERFORMING ORGANIZATION REPORT NUMBER
9. SPONSORING/MONITORING AGENCY NAME(S) AND ADDRESS(ES)	10. SPONSOR/MONITOR'S ACRONYM(S)
	11. SPONSOR/MONITOR'S REPORT NUMBER(S)

12. DISTRIBUTION/AVAILABILITY STATEMENT
Approved for public release; distribution unlimited

13. SUPPLEMENTARY NOTES

14. ABSTRACT

15. SUBJECT TERMS

16. SECURITY CLASSIFICATION OF:			17. LIMITATION OF ABSTRACT	18. NUMBER OF PAGES	19a. NAME OF RESPONSIBLE PERSON
a. REPORT **unclassified**	b. ABSTRACT **unclassified**	c. THIS PAGE **unclassified**	**Same as Report (SAR)**	**6**	

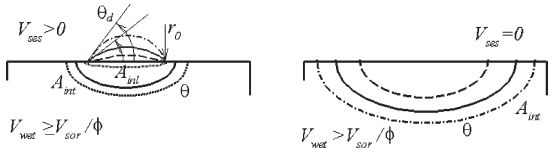

Figure 1. Schematic of the sessile droplet sorption, including the definitions of inlet A_{inl} and interface A_{int} boundary, dynamic θ_d, and liquid|solid θ contact angle for sessile volume V_{ses}: (a) greater than and (b) equal to zero.

The determination of multiphase flow parameters: capillary pressure and relative permeability have been described by Navaz et al. for the blister agent bis(2-chloroethyl) sulfide and agent simulants on a range of porous substrates.[24]

The experiments in this article were carried out with the nerve warfare agent, *O*-ethyl *S*-(2-diisopropylaminoethyl) methylphosphonothiolate (VX), sorbing into medium-grain sand. The sessile-drop volume, wetted imprint surface area, and penetration depth were measured in time. The time in which the experimental results were collected was much longer than the time it takes for sessile drop to sorb into the sand. In this way, the numerical and experimental results are compared over a large number of experimental points rather than for one experimental point (i.e., the time it takes for liquid to infiltrate a porous medium). The multiphase sorption influences other transport rates such as evaporation, reaction, and the agent fate significantly.[25,26] Given the large number of liquid/substrate combinations, it is useful to develop a predictive computational model to obtain insight into this process. Such a model would be applicable to pesticides, industrial chemicals and have environmental, defense, and homeland security implications.

2. Model System

An initial sessile drop volume $V_{ses}(t_0)$ of liquid is deposited onto the porous medium surface, where in the sorption process, the instantaneous volume $V_{ses}(t)$ remaining on the surface decreases, and sorbed volume $V_{sor}(t)$ increases in time. The sorbed liquid wets the porous substrate of p*orosity* ϕ, where ϕ is the ratio of void-space volume to total volume. The wetted imprint volume is equal to $V_{wet} = V_{sor}/\phi$ for fully saturated sorption, or $V_{wet} > V_{sor}/\phi$ for nonsaturated sorption. The spread and sorption are driven by a capillary force, and even when there is no liquid left on the porous medium surface $V_{ses}(t) = 0$, the sorption continues and (V_{wet}) increases in time with the volume saturated by the liquid decreasing at the same time. The capillary force is responsible for the shapes of the sessile-drop and the wetted imprint, and a coupled problem of flow in the surface liquid together with the flow in porous substrate has to be solved. In some special cases, such as constant droplet base radius, the flow problem solution in the sessile volume is known, and only the flow within the porous substrate needs to be determined. Figure 1 shows the liquid fate during the spread and sorption into a porous substrate for the special case of the constant droplet base radius (r_0). The region where liquid sorbs into the medium is defined as the inlet boundary area, A_{inl}. The region where the liquid front advances through the substrate is defined as the liquid interface area, A_{int}. The dynamic contact angle θ_d changes in time and is defined as an angle between porous medium surface and tangent at the sessile droplet shape from the contact line. This differs from the contact angle within the porous medium, θ defines the angle of wetted and nonwetted-regions and remains the same throughout the sorption process.

The liquid flow in the porous substrate is formulated as a multiphase flow problem for gas and liquid phases. The problem is described by coupling continuity equation, Darcy's Law, the capillary pressure jump condition at the gas/liquid interface,[23] and the sum of phase saturations (s_{Gas}) and (s_{Liq}):

$$\nabla \cdot s^{[i]}\rho^{[i]}\mathbf{u}^{[i]} = 0 \tag{1}$$

$$\mathbf{u}^{[i]} = -\frac{K_p^{[i]}}{\mu^{[i]}}\nabla(p^{[i]} - \rho^{[i]}\mathbf{g}\cdot\mathbf{x}) \tag{2}$$

$$p_c = p_{Gas} - p_{Liq} \tag{3}$$

$$s_{Gas} + s_{Liq} = 1 \tag{4}$$

where [*i*] can be either the gas or liquid phase of viscosity μ and phase permeability K_p. The phase velocity u and pressure p are obtained from eqs 1-4 with the capillary pressure p_c equal to the pressure difference of nonwetting and wetting phases. The instantaneous position of the free interface area A_{int} is determined from the liquid phase velocity. The change of the wetted volume V_{wet} in time is calculated after integrating the liquid phase flow over A_{int}:

$$dV_{wet}/\,\mathrm{d}t = \int_{A_{int}} \mathbf{u}_{int}^{[Liq]}\,\mathrm{d}A \tag{5}$$

Except for the surface of substrate on which the droplet is deposited, all other boundaries are defined as no-flow for either phase. This condition transforms into a zero-pressure gradient in the direction normal to the boundary. For the boundary on which the sessile volume resides, the gas phase flows out from the porous substrate domain and through the boundary fraction that is not covered by liquid. It is important to note that only a part of this boundary is covered by liquid, defined by A_{inl} in Figure 1. The gas pressure is equal to the atmospheric pressure p_{atm}, and there is no liquid flow across this surface. At A_{inl}, the liquid pressure is equal to the pressure within the sessile droplet, and there is no gas flow across the area defined by A_{inl}. Once there is no sessile liquid left $V_{ses} = 0$, gas pressure becomes equal to p_{atm} over all domain boundaries, and liquid pressure at the free interface is calculated from eq 3.

The capillary pressure in eq 3 is calculated from the Leverett function, scaled by substrate porosity ϕ, single-phase flow permeability K_{sp}, and contact angle θ. The phase permeability K_p of each phase is expressed from K_{sp} and the relative permeability k_r that is a quadratic function of saturation. The details of the parameter determination and numerical method based on the continuum approach is described in Navaz et al.[24] In brief, the governing equations describing mass and momentum conservation (eqs 1 and 2) for liquid and gas phases are written over a small volume and then assembled and solved for overall computational domain. The partial differential equations in a continuum domain are solved on a finite-difference mesh with fourth-order Runge−Kutta explicit numerical scheme used for time integration. The algorithm is second-order in space and fourth-order in time. The numerical solution includes each phase saturation, pressure

(24) Navaz, H. K.; Markicevic, B.; Zand, A.; Sikorski, Y.; Chan, E.; D'Onofrio, T. G. *J. Colloid Interface Sci.* **2008**, *325*, 440−446.
(25) Roberts, I. D.; Griffiths, R. F. *Atmos. Environ.* **1995**, *29*, 1307−1317.
(26) Griffiths, R. F.; Roberts, I. D. *Atmos. Environ.* **1999**, *33*, 3531−3549.

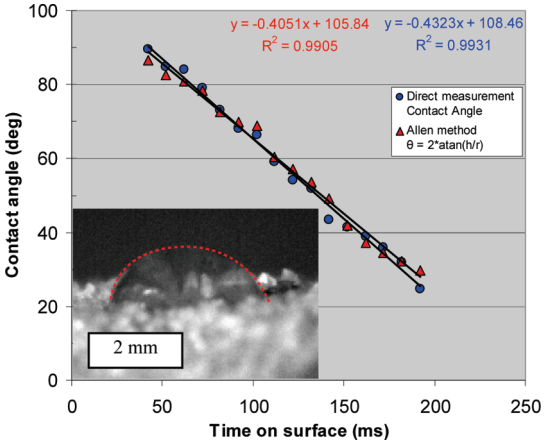

Figure 2. Change of the dynamic contact angle θ_d of VX sessile droplet on a medium-grain sand. Inset image shows the sessile droplet for time t = 73 ms after freefall impact. A red outline is provided for image clarity, and the width of the white box represents 2 mm.

and velocity, and how each changes in time. From the solution, other time-dependent characteristics can be obtained, including wetted volume, area of imprint, and protrusion depth into substrate. Initially, the numerical solution is validated against experimental results by comparing the time it takes for volume to infiltrate porous substrate, and a very good agreement was documented.[24]

3. Experimental Procedures

Caution! The handling of chemical warfare agents should only be performed by trained personnel at an approved facility using applicable safety, security, and surety precautions.

A medium grain-size sand AFS-50, 98% SiO_2 acquired from Warmwell quarry (Bardon Aggregates) with the following properties: density of 2.65 g/cm^3, BET surface area of 0.33 m^2/g, and grain size between 0.25 mm and 0.50 mm was used in experiments. The samples of nerve warfare agent O-ethyl S-(2-diisopropylaminoethyl) methylphosphonothiolate (VX) were taken from existing stocks and were determined to have a purity of at least 90.3%. To each stock aliquot of VX, 3 wt %/wt diisopropylcarbodiimide (Fluka) stabilizer was added to simulate a munitions-grade VX stock. In all experiments, a droplet of initial volume equal to 6 mm^3 was deposited onto sand. In the set of experiments, the spread and sorption time characteristics, including (i) dynamic contact angle θ_d, (ii) imprint surface wetted area A_w, and (iii) penetration depth d_p, were measured, as described below.

For the dynamic contact angle measurements, the VX was deposited as a 6 mm^3 droplet using a micropipet (Hamilton 10 μL adjustable pipet, model 1708−32) allowing the droplet to freefall, rather than to be ejected forcefully. Since the infiltration rate of the sessile volume into sand is fast, a high-speed video camera (MotionXtra HG-TH, Redlake, 1000 frames/s) was used to capture freefall velocity, contact angle, and sessile droplet lifetime on the sand. Contact angle measurements, θ_d, and droplet volume calculations were obtained using custom Matlab routines from a series of side-on sessile volume images, as shown in Figure 2.

Wetted area and penetration depth measurements were carried out using the apparatus shown in Figure 3, both schematic (left) and actual design (right). The sand container top surface has interior dimension of 9.2 cm × 3.3 cm, enabling the deposition of multiple drops. The surface spread area A_w was captured using a video system (Sony XC-ST50, Imperx capture card, custom software by Battenkill Technologies) at a rate of once per 3 min. The penetration depth d_p images were captured using a digital SLR camera (Canon digital Rebel EOS SLR, Canon control software), with frames captured once per minute. Images were analyzed for the area, eccentricity, and equivalent diameter using a custom-written Matlab routine. The code used a combination of auto-thresholding and morphological processing routines to identify the droplet. The construction of the sand container enables the placement of the camera underneath the apparatus such that it does not interfere with the sorption process.

Once identified, the geometric parameters were calculated. Movie frames were rendered of the original results with an overlay of the perimeter boundary, to enable visual comparison between the original image and calculated boundary. An example of a processed movie frame for A_w is shown in Figure 3 (top-down image). To facilitate determining d_p, the construction of the sand container with inclined bottom wall creates a substrate of continuously variable and known depths. The top-down camera measures the spread dynamics of the drop on the surface A_w, while the bottom-up camera determines penetration time by color change of the M8 chemical warfare agent detector paper, placed at the bottom of the incline before adding the sand. The depth of penetration d_p is calculated from the known slope of the bottom wall, $\alpha = 7°$, and the distance of the initial color change measured from the box leading edge. Examples of top-down and bottom-up images (right) used to determine A_w and d_p are included in Figure 3. Finally, for the droplets for which VX did not reach the indicator paper, the wetted imprints were taken out from the sand, and from their images, the imprint shape was calculated.

4. Results and Discussion

From the experimental results, the time characteristics of the dynamic contact angle θ_d, imprint wetted area A_w, and penetration depth d_p are calculated. The change of θ_d in time is calculated for one droplet only. The characteristic $A_w(t)$ and a single value of d_p were measured for each droplet applied. The experimental results are compared with the numerical predictions. In the numerical solution, the density, dynamic viscosity, and surface tension of VX are set $\rho = 1.01$ g/cm^3, $\mu = 1.23 \times 10^{-2}$ Pa × s, and $\sigma = 3.2 \times 10^{-2}$ Pa × m. The medium grain-size sand porosity and permeability are determined to be equal to $\phi = 0.44$ and $K = 6.05 \times 10^{-11}$ m^2.[27] The values of the capillary pressure p_c and relative permeability k_r are given by Navaz et al.[24]

The droplet fell a distance of 2.3 mm within 18 ms, and was observed to remain as spherical during the descent using the high-speed imagery. Because of impact on the surface, oscillations were observed within the droplet for the initial 30 ms after impact. Hence, the dynamic contact angle θ_d is measured starting at 40 ms after the impact. The Weber number is defined as the relative ratio of kinetic to surface energy. This number can be calculated from the impact velocity (around $u_{im} \approx 0.2$ m/s) and the characteristic length (the diameter of free falling droplet, d_{dr} = 2.254 mm) according to $We = \rho u_{im}^2 d_{dr}/\sigma$ which is around $We \approx 3.5$. This relatively low number indicates that the droplet impact velocity did not overcome the surface energy, a finding further supported by the nondistorted spherical shape of the free-falling droplet. The sessile-drop volume after 40 ms was calculated to be 5.9 mm^3, implying that no significant volume sorbed into the sand in this initial time interval compared to the initial volume of 6.0 mm^3. The volume is calculated from the height and footprint diameter of the sessile drop with $V = 1/3\pi h^2(^3/_2 d - h)$, with a typical error of ±10%. In Figure 2, the results of measured θ_d are shown for time up to $t = 192$ ms. Measurements were not taken once $\theta_d = 25°$ as sand grains are comparable in size with the sessile droplet height that would produce large errors in θ_d calculated. For shorter times and sessile droplet heights being larger, the sessile

(27) Zand, A. R.; Sikorski, Y.; Sanders, M.; Navaz, H. K. *J. Phys. Nat. Sci.* **2007**, 1.

 DOI: 10.1021/la903071q C

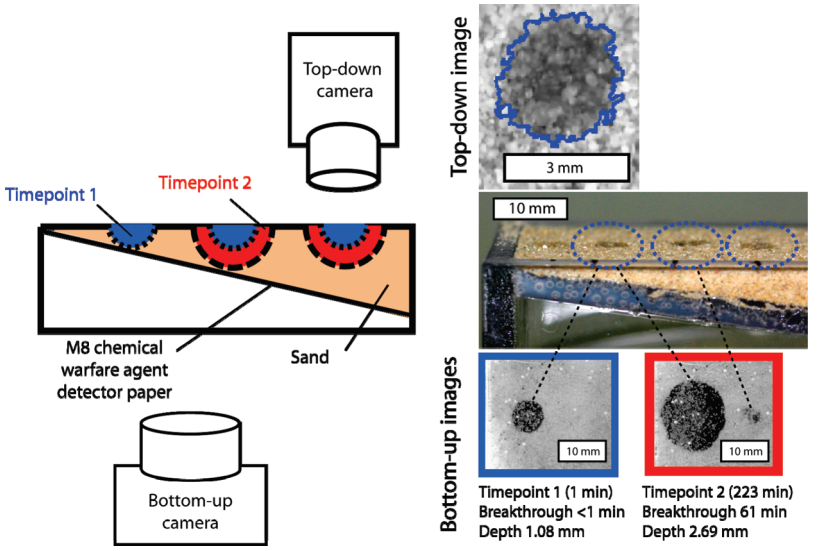

Figure 3. Experimental setup and imprint shape measurements: principle of penetration depth apparatus (left) and an actual apparatus photograph (right). The images of wetted imprint area (top right) and breakthrough point were captured by indicator paper (bottom right).

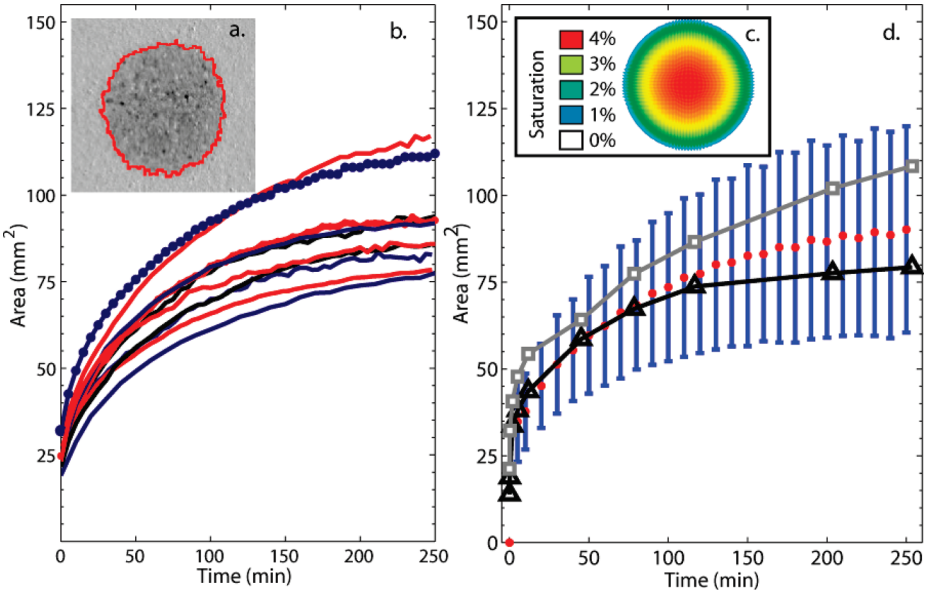

Figure 4. Summary of wetted imprint surface area A_w results: (a) typical frame and its overlaid contour (red line) used to measure A_w, (b) individual experimental results $A_w(t)$, (c) numerical solution, and (d) experimental averaged $A_w(t)$ and confidence interval ($\pm 2\sigma_{Aw}$) given by full symbols and error bars, and numerically calculated $A_w(t)$ for 1% (empty squares) and 2% (empty triangles) saturation threshold.

droplet shape can be clearly distinguished as can be seen from the inset in Figure 2, for $t = 73$ ms. In Figure 2, θ_d is determined using two methods: (i) direct measurement of the angle between the substrate and the droplet outer shape finding the tangent line, and (ii) calculated from the ratio of the drop height h to radius of the base r_0, where $\tan(\theta_d/2) = h/r_0$.[28] The agreement between two methods is excellent (circles and triangles in Figure 2), where from both methods it is found that there is a linear decrease in the contact angle of 0.4°/ms. The ratio method is appropriate only for sessile droplet in the form of a spherical cap. The observed agreement between two methods implies that VX on medium grain-size sand indeed forms spherical cap geometry. The sessile droplet sorption time is also predicted numerically, where the influence of deposition velocity is neglected and the droplet base radius r_0 remains constant. The numerically calculated value, 625 ms, compares excellent with the experimentally measured sorption time, 613 ms.

Once the sessile VX has sorbed into the sand, a further wetting of sand by VX occurs as the agent sorbes into previously nonwetted volume. Thus, both A_w and d_p increase further in time. The experimental and numerical trials are carried out up to 250 min. The results reveal that the imprint wetted area A_w ranges from 20 mm^2 to 110 mm^2, and penetration depth d_p from 1 mm to 4 mm. Thus, an increase more than four times for both A_w and d_p is observed, giving VX saturation s reduction for over an order of magnitude ($s < 0.1$). The droplet experiment was repeated ten times obtaining ten distinct $A_w(t)$ curves, from where the results repeatability is analyzed. From these experiments, the average wetted area after $t = 200$ min is 89 mm^2, with a standard deviation of 13 mm^2 and a relative standard deviation of 15%.

(28) Allen, J. S. *J. Colloid Interface Sci.* **2003**, *261*, 481−489.

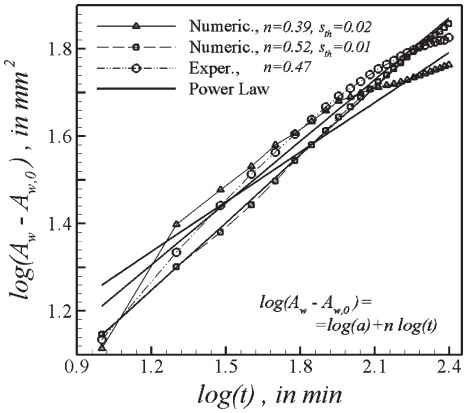

Figure 5. Power law comparison for two numerical (s_{th} = 1% and s_{th} = 2%) and the experimental wetted area results. The changes in powers n show that the threshold saturation is in the range of between 1% and 2%.

The variation in d_p was also observed. It should be noted here that there are two sources of the variability of the experimental data. One is from the experimental error and second one is from the sand structure. Because of the droplet size and pore size distribution in the sand, depending on where the droplet is placed, the liquid surface flow (large pores beneath the droplet), or liquid protrusion flow (small pores) can be favored. This is corroborated by experimental results for d_p, where after t = 1 min, in two different experiments d_p was found equal to 0.7 mm and 1.1 mm, respectively.

Figure 4 summarizes both experimental and numerical results for A_w. The wetted imprint area is determined from experimental images (part a), used to calculate the wetted area. The individual experimental results are shown in Figure 4b. In all cases, A_w increases rapidly, and then levels off as A_w approached the maximum spread. The individual experiments were self-consistent and smooth compared to the test-to-test variance. The numerical results are shown in Figures 4c and 4d. The colors in Figure 4c indicate the level of saturation for VX in the sand as a function of spatial position. The saturation is defined as a fraction of pore volume occupied by liquid VX. The average A_w is shown in Figure 4d with full red circles, and bars represent the 95% confidence interval ($\pm 2\sigma_{Aw}$). It should be mentioned here that the experimentally measured A_w, obtained from image processing, does not provide information on the saturation level of the medium, nor is the threshold value known for differentiating wet versus dry. However, in the numerical solution, this saturation threshold for the wetted surface visibility was set at 1% and 2%, with $A_w(t)$ profiles represented by square and triangle symbols in Figure 4, respectively. The numerical results indicate that setting the saturation threshold smaller gives a larger wetted area, with both numerical solutions (1% and 2% threshold saturation) within confidence interval of $A_w(t)$ computed from the experimental results.

The numerical results from Figure 4 show that the change of the wetted area depends on the threshold saturation (s_{th}) which is defined as a minimum saturation for which the sand becomes visibly wet (recordable by camera). The experimental results are between the 1% and 2% saturation threshold curves that are obtained by numerical solution. For all three profiles $A_w(t)$, the wetted area initially increases more rapidly compared to later times. However, for the longer spread time, the experimental and one of the numerical results (s_{th} = 2%) for the wetted area reach almost a constant value. It takes a longer time for the 1%

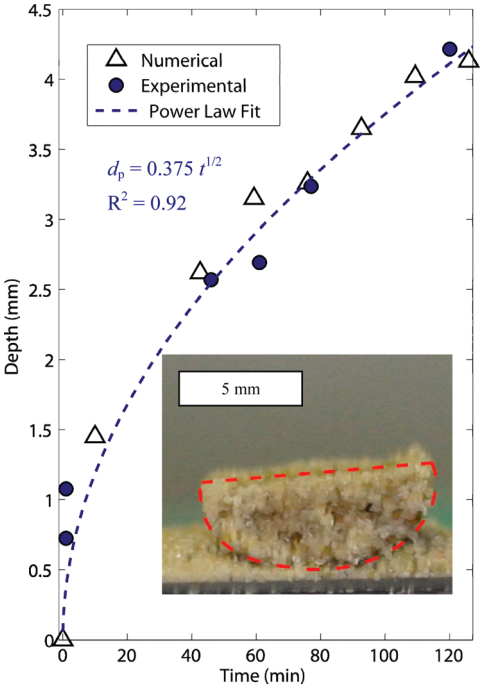

Figure 6. Changes of penetration depth as a function of time $d_p(t)$ including experimental values (full circles), numerical predictions (empty triangles), and square root $d_p(t)$ dependence (dashed line). The shape of wetted imprint and length scale (5 mm) are shown in the inset.

saturation threshold wetted area curve to demonstrate the same behavior. In order to investigate these changes, the wetted area results are analyzed using a power law:

$$A_w(t) - A_{w,0} = at^n \quad (6)$$

where $A_{w,0}$ is the wetted area right after the sessile volume becomes equal to zero, and a and n are the power law constants. The results for $A_w(t)$ as obtained from the numerical solutions (s_{th} = 1% and s_{th} = 2%) and experiments are shown in a log−log plot in Figure 6, using different symbols. The symbols are connected with thin lines for better visibility. The thick solid lines represent the power law linear regression from eq 6. The powers $n \approx 0.47$ and $n \approx 0.39$ are determined for the experimental and the numerical results of 2% saturation threshold wetted area, respectively. Setting the saturation threshold to s_{th} = 1%, the numerical $A_w(t)$ (square symbols) follows the power law in the whole time range with $n \approx 0.52$. This implies that the threshold saturation is chosen properly, and its value is in the range 1% < s_{th} < 2%. From the same numerical solution as shown in Figure 4b, the penetration depth $d_p(t)$ is also calculated.

The comparison between experimental and numerical results is given in Figure 5 with circular and triangular symbols, respectively. The numerical values of $d_p(t)$ are computed for saturation threshold equal to 1%. It can be seen that the numerical results closely follow the experimental data. The numerical solution curve $d_p(t)$ is not smooth, caused by a computational grid. Since there is smaller number of computational nodes in the penetration depth direction, the nodes with saturation less than the saturation threshold are truncated and some small "jumps" in the $d_p(t)$ profile are observed. In calculating the $A_w(t)$ profile, there are a larger number of nodes and smooth numerical $A_w(t)$ is calculated. For the experimental cases in which VX does not reach the indicator paper placed at the sand apparatus bottom, the wetted

 DOI: 10.1021/la903071q E

imprint is removed from the sand and photographed as an illustration of the wetted-imprint shape. The image of one of those imprints is shown in the inset in Figure 5. Additional investigation of the imprint shape reveals that the imprint is a spheroid in shape; the result that is observed from the numerical solution also. However, it is important to note that the d_p is not measured from these wetted imprint shapes, as there may be liquid present outside the region, but not enough for induce clumping. The protrusion depth is modeled as a power function of time, where it is found that d_p is a time square root function, represented by dashed line in Figure 5. Finally, the square root dependence d_p of time t has been reported[8,29] for the dynamics of the capillary driven flows into porous substrates.

5. Conclusions

The experimental method to measure the dynamics of the chemical warfare agent VX sorption into medium grain-size sand for both sessile droplet present and after no liquid is left on the porous medium surface is developed. The sessile volume sorption rate and shape are determined using the high-speed video camera, where the sessile droplet is in the shape of spherical cap, and the dynamic contact angle decreases in time linearly. The wetted imprint is a spheroid in shape with its base referred as wetted imprint area and other axis defined as penetration depth. Both of these quantities are measured experimentally by recording the surface wetted area and identifying the arrival time of VX to the sand bottom of known depth. The imprint volume increases faster initially compared to the longer times, and the penetration depth can be expressed as a square root function of time. The infiltration process is also solved numerically, in which besides liquid and porous medium physical properties, the multiphase flow transport parameters capillary pressure and phase permeability need to be known. All three characteristics: (i) dynamic contact angle, (ii) imprint wetted area, and (iii) penetration depth are computed and compared with experimental results with a very good agreement found over the whole time interval during the sorption occurs. These numerical and experimental methods can be used to determine the spread and sorption of hazardous materials into a variety of substrates. Such studies are applicable to pesticides, industrial chemicals and have environmental, defense, and homeland security implications.

Acknowledgment. The authors thank the Air Force Research Laboratory, Human Effectiveness Directorate, Biosciences and Protection Division, Wright-Patterson AFB, Ohio, and the US Army Edgewood Chemical Biological Center, Aberdeen Proving Ground, Maryland for their support of this effort. We specifically thank Dr. James Savage, Dr. H. Dupont Durst, Mr. William Kilpatrick, and our consultant, Mr. Joseph Kiple, for their support throughout this project. Dr. D'Onofrio thanks DTRA for funding support through the Environmental Fate of Chemical Agents Program (BA07TAS041), Dr. David Tevault and Mr. Wendel Shuely for helpful discussions, and Mr. Jack Molnar for assistance with the construction of the sand exposure system.

(29) Rivin, D.; Lindsay, R. S.; Shuely, W. J.; Rodriguez, A. *J. Membr. Sci.* **2005**, *246*, 39−47.